The Friedlander–Heaviside series for describing pressure-time history of reflected blast waves

Luiz Bortolan Neto [a, b]

luizb@ansto.gov.au

[a] *Australian Nuclear Science and Technology Organisation (ANSTO), Locked Bag 2001, Kirrawee DC NSW 2232, Australia*

[b] *DMTC Ltd, Level 2, 24 Wakefield St, Hawthorn VIC 3122, Australia*

Abstract

The detonation of an explosive charge within a building or confined space will often result in reflected blast waves off the surrounding structure. Even though an extensive number of studies have examined this problem, only simplified mathematical descriptions of the pressure-time history are available. As these descriptions lack the fidelity required for detailed analysis of structural response to reflected blast loading, engineers and designers often must rely on expensive and resource intensive test data and validated numerical simulations to estimate dynamic structural loading. Other approaches which use pressure-impulse approximations provide reasonable predictions for estimating the global mechanical response of a structure, but they are unsuitable for evaluating localised structural failure. The Friedlander–Heaviside series is here introduced for describing the full dynamic overpressure-time history of reflected blast waves. This series provides a reasonably simple formulation that can describe with high accuracy the sequence of pressure peaks observed in pressure-time history curves from reflected blast waves. The Friedlander–Heaviside series is constructed by applying the superposition principle to a number of individual pulses formed by combining the well-known Friedlander equation with the Heaviside step function. Examples from the literature are used to validate the Friedlander–Heaviside series for describing pressure-time history of reflected blast waves. Once the required parameters have been established, the Friedlander–Heaviside series can then be readily applied in conjunction with advanced structural models for obtaining detailed evaluations of structural response to reflected blast loadings.

Keywords: Reflected Blast Waves, Reflected Shockwaves, Pressure-Time History, Friedlander Equation, Friedlander–Heaviside Series

Nomenclature

A_Ω	vent cross-sectional area
C	Weibull constant
$\mathrm{H}(\cdot)$	Heaviside step function
k	fitting parameter
m_e	mass of the explosive charge
$\overline{m}$	mass of the blast products gaseous mixture
n	number of relevant peaks
p	pressure
p_a	ambient pressure
$\hat{p}$	peak incident pressure
p_{qs}	gauge quasi-static pressure
$\hat{p}_{qs}$	peak gauge quasi-static pressure
$\overline{p}$	residual internal pressure
Q_e	explosive specific energy
t	absolute time
$\hat{t}$	time of arrival
t^+	time at which the positive phase ends
$\check{t}$	time at which the local pressure pulse is no longer valid
t_0	time at which the initial conditions are still valid
v_Ω	outflow velocity through the vent
V_a	ambient/internal volume
V_e	volume of the explosive charge
α	decay coefficient
β	positive phase decay rate parameter
γ	adiabatic index of the ambient air
$\overline{\gamma}$	adiabatic index of the blast products gaseous mixture
η	Weibull exponent
ρ_a	ambient density
ρ_e	density of the explosive charge
$\overline{\rho}$	residual internal gas density
ψ	dynamic overpressure
$\hat{\psi}$	peak incident overpressure
$\check{\psi}$	leveling static overpressure
τ	local time
τ^+	positive phase duration
$\check{\tau}$	duration of the local dynamic overpressure pulse
Ω	vent domain

Subscripts

a	ambient
e	explosive
i	peak index
qs	quasi-static

1 Introduction

Understanding the potential damage caused by explosions is of extreme importance when investigating structures and devices that can minimise the harm inflicted to individuals and assets. The threat posed to buildings in urban environments and to military platforms is particularly pertinent as these are the most usual targets. A considerable number of experimental and numerical studies have been devoted to the analysis of blast wave reflection [1, 2] and to the evaluation of explosions in built environments [3-11] and in unvented and vented confined spaces [12-27].

Explosions in complex urban settings and in confined spaces are more intricate than those in open fields as multiple shockwave reflections are often present [11, 22]. Explosions in confined spaces are also termed internal blast. In internal blast loading cases, the initial peak overpressure is followed by less intense peaked overpressures until settling to a quasi-static overpressure that eventually reduces to the ambient pressure if sufficient venting has become available. The quasi-static overpressure can remain for a considerable period until fully dissipated, or vented, from confined structures.

Even though knowledge of the quasi-static pressure can provide adequate predictions of the global response of structures subjected to internal blast loading [22], precise near field predictions require knowledge of the dynamic overpressure and peak pressures profile as they are determinant in the development of some localised failure and can improve estimates of the global mechanical response. Additionally, the dynamic overpressure is the main cause of damage of structures in built environments [7]. For those reasons, predicting damage based solely on the initial peak pressure can be deceptive as blast load duration along with subsequent pressure peaks are just as important when evaluating structural damage [22].

The pressure-time history is usually obtained from experiments or from validated computational fluid dynamics (CFD) simulations. Resource restrictions, high associated costs, and long lead times from conception to testing make data collection from blast testing relatively complicated and restricted to localised gauging sensors [28]. To obtain a complete description of the reflected blast flow, CFD simulations usually couple the conservation laws from Euler's system of hyperbolic partial differential equations (PDE) for adiabatic and inviscid flow with the Jones–Wilkins–Lee (JWL) equation of state for explosive products [29]. The numerical solution of this system of PDEs is not trivial and suitable discretisation in space and time must be employed to ensure optimal results [30], which may require days of computer processing time [31]. As a trade-off to the long turnaround times from blast testing and CFD simulations, rich and detailed information is captured. Nonetheless,

preliminary studies and evaluations of explosive loads can benefit from conservative and high confidence swift solutions of simplified phenomenological and analytical approaches.

Despite the extensive research dedicated to understanding reflected blast waves, the specialised literature provides only a few semi-empirical and simplified analytical models for estimating the residual gauge quasi-static pressure [12-14] and extremely simplified descriptions of the pressure-time history based on pressure-impulse loading [17-19]. The Friedlander equation [32] has been extensively employed for describing pressure-time histories from blast waves in open fields [33]. Surprisingly, no effort has been dedicated to extending the Friedlander equation to the analysis of reflected blast waves.

In the present paper, the dynamic overpressure of reflected blast waves is assumed to behave in a physically linear fashion, in accordance with the superposition principle. Owing to the additive properties of this principle, the dynamic overpressure can then be conceptually constructed by combining several Friedlander waveforms (pulses) in sequence, with the information from each pulse being conveniently activated or deactivated by a corresponding Heaviside step function. This combination yields a so-called Friedlander–Heaviside series that can describe reasonably well the dynamic overpressure-time history of reflected blast waves. The theory utilised for deriving this series is detailed in Sections 2 and 3. In Section 2 the Friedlander theory of blast waves in open fields is reviewed, giving particular attention to the Friedlander waveform. The mechanical behaviour of reflected blast waves and the required assumptions utilised to develop a workable solution are discussed in Section 3. This section also reviews models for estimating the quasi-static pressure of confined blast cases before formally introducing the Friedlander–Heaviside series formulation. Application of the Friedlander–Heaviside series to three different scenarios in Section 4 demonstrates the capacity of this formulation to furnish accurate descriptions of the dynamic overpressure-time history.

2 Blast waves in open-air

Blast waves are generated from the sudden energy release from explosive devices, resulting in a supersonic expansion of compressed gases. The leading shockwave is trailed by a self-similar subsonic flow field. Measurements of the hydrostatic pressure-time history of blast waves have been possible with the introduction of piezo-electric transducers and associated amplifiers in the 1940s. During this time the Friedlander equation was also introduced as a means of promptly describing these time histories [32, 33].

Blast waves in open-air are characterised by the absence of interactions with surfaces and obstacles that can cause absorption, reflection, diffraction, and refraction. Without interferences, the

propagating shockwave gradually degenerates into a soundwave [33]. The original Friedlander equation can describe reasonably well this type of blast waves, only requiring measurements of the peak overpressure and positive duration. Figure 1 illustrates the pressure pulse described by the Friedlander equation (1). Even though a global coordinate system can be used, it is customary to define the Friedlander equation in terms of local coordinates with the origin set at the intersection between time of arrival and ambient pressure. Local variables are the local time τ, duration of the positive phase τ^+, overpressure ψ, and peak overpressure $\hat{\psi}$. Global variables include time t, time of arrival $\hat{t}$, time at which the positive phase ends t^+, pressure p, peak pressure $\hat{p}$, and ambient pressure p_a.

$$\psi(\tau) = \hat{\psi}\left(1 - \frac{\tau}{\tau^+}\right)\exp\left(-\frac{\tau}{\tau^+}\right) \tag{1}$$

The Friedlander equation (1) may be converted to global coordinates with the following relationships:

$$\tau = t - \hat{t}, \quad \tau^+ = t^+ - \hat{t}, \quad \psi = p - p_a, \quad \hat{\psi} = \hat{p} - p_a \tag{2}$$

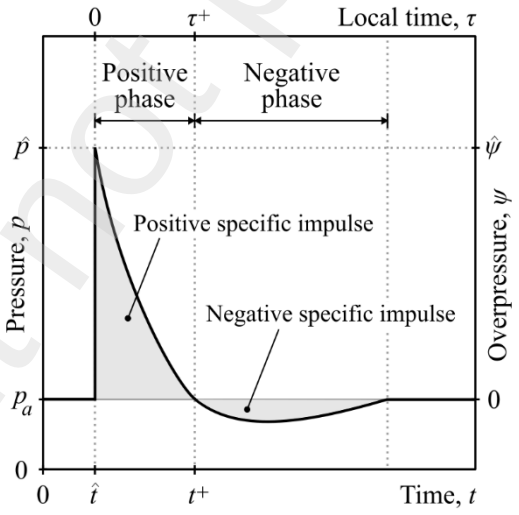

Figure 1. Typical Friedlander pressure-time history characteristic of high explosives detonating in free fields. The local coordinate system has its origin at the intersection between the time of arrival and the ambient pressure.

In some conditions the original Friedlander equation cannot accurately describe the shape of the blast waves at short radial distances, specifically in the case of trinitrotoluene (TNT) and pentolite explosive charges [33]. To address this problem, modified versions of the Friedlander equation have

been proposed whereby a decay coefficient or a positive phase decay rate parameter is included in the exponent to improve precision. With the addition of the decay coefficient α, the Friedlander equation becomes

$$\psi(\tau) = \hat{\psi}\left(1 - \frac{\tau}{\tau^+}\right)\exp\left(-\alpha\frac{\tau}{\tau^+}\right) \quad (3)$$

By including the positive phase decay rate parameter β, the Friedlander equation is rewritten as

$$\psi(\tau) = \hat{\psi}\left(1 - \frac{\tau}{\tau^+}\right)\exp\left(-\beta\tau\right) \quad (4)$$

Investigations comparing the performance of Eq. (3) against Eq. (4) have shown that the fitted coefficients $\hat{\psi}$ and τ^+ might be similar but not identical and that often β does not match α/τ^+ [33, 34]. These investigations have found, in general, greater accuracy using the modified Friedlander equation (4) [33]. For particular cases where $\alpha = 1$ and $\beta = 1/\tau^+$, the modified versions revert back to the original Friedlander equation.

3 Reflected blast waves

After the intense release of energy from explosives in areas surrounded by surfaces and obstacles, the resulting initial expanding shockwave will drive a discontinuous flow of compressed gaseous blast products. Upon reaching and interacting with nearby structures, some of the shockwave kinetic energy is absorbed and the residual kinetic energy drives the shockwave reflection. This process is repeated continuously until there is not enough kinetic energy available in the system. Even though the entire energy dissipation process can persist for a relatively long time, reflections with high amplitudes last for a very short period and are then followed by a quasi-static state.

The initial blast detonation in a confined or urban environment is typically followed by reflected shockwaves. Figure 2 illustrates the pressure-time history of reflected blast waves from three different situations. If the detonation happens at an open area with several obstacles, such as built environments, the reflected blast waves will fade gradually, eventually stabilising at the ambient pressure level p_a (Fig. 2a). In the case of confined blast loading, the multiple reflected blast waves will interact with the overall structure, subduing to a quasi-static state whereby a nearly constant residual overpressure $\overline{p}$ remains until its dissipation is possible (Fig. 2b). Confined blast loadings in vented or breached structures exhibit reflected blast wave interactions concurrent to slowly decaying pressure until levelling with the ambient pressure (Fig. 2c). The magnitude variation with

time of the quasi-static pressure relief depends on the internal volume of the structure and venting/breached area.

In confined blast loading cases, an accurate approximation of the quasi-static pressure is of particular interest as it strongly influences the global response of the structure [22, 35]. Knowledge of the pounding internal peak pressure and subsequent shock reflections is also necessary for obtaining precise estimates of the resulting structural damage and deformation [22].

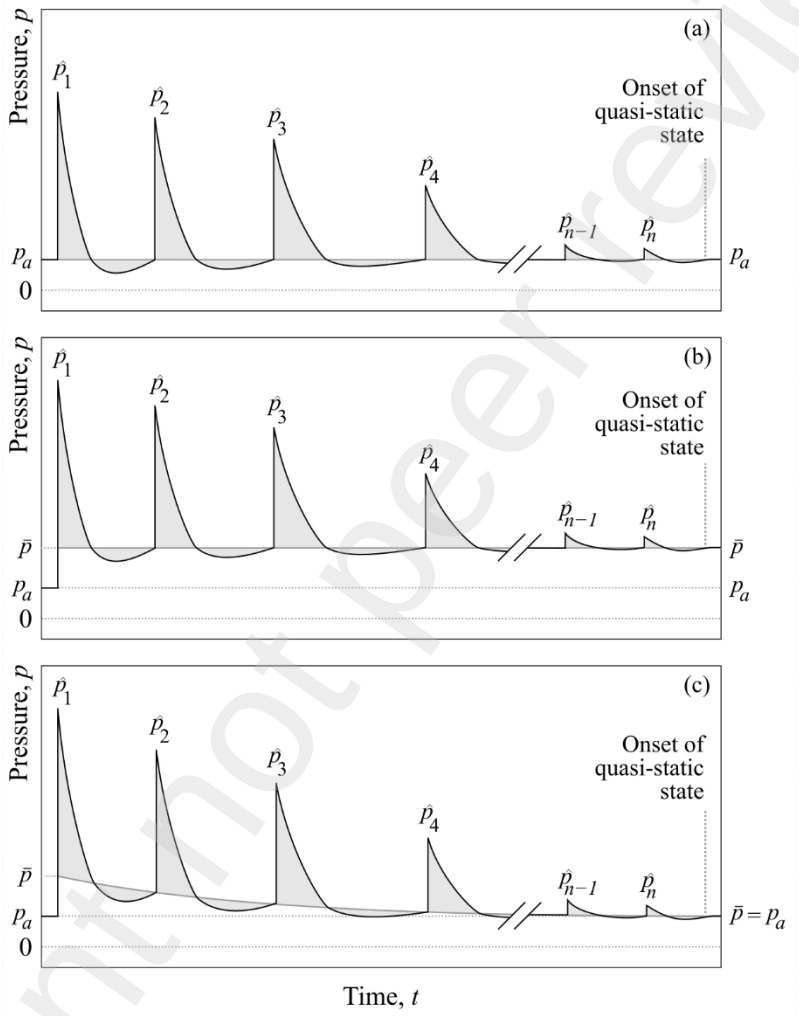

Figure 2. Schematic of pressure-time history for reflected blast waves in (a) open area with obstacles, (b) unvented/non-breached confined structure, and (c) vented/breached confined structure.

The dynamic overpressure is here defined as the pressure exceeding the ambient and quasi-static pressure. For this reason, determining the quasi-static pressure is necessary for establishing an independent model for describing the pressure-time history of reflected blast waves. Both empirical and simplified analytical models are available in the specialised literature for estimating the peak quasi-static overpressure of confined structures with and without venting. The most relevant models

are reviewed in the next section, which is followed by the introduction to the Friedlander–Heaviside series for describing reflected blast waves.

3.1 Quasi-static pressure from internal blast loadings

Calculating the residual pressure is important for determining the onset of the quasi-static state. It can also be used to separate the dynamic overpressure from the total pressure profile. The residual pressure for a confined explosion $\overline{p}$ is here defined as the combination between the ambient pressure p_a and the gauge quasi-static pressure p_{qs}, which can be expressed as

$$\overline{p}(t) = p_a + p_{qs}(t) \tag{5}$$

For detonations in open spaces the gauge quasi-static pressure is negligible, which gives $p_{qs}(t) = 0$. The gauge quasi-static pressure in confined spaces is usually determined from empirical formulae [12, 13]. More recently, a simplified analytical approach has been proposed [14]. These models are reviewed below as they can be readily combined with the dynamic overpressure-time history described by the Friedlander–Heaviside series (Section 3.2) to provide the complete pressure-time history.

3.1.1 Empirical relationships

Weibull [13] derived a simple empirical power-law relationship to estimate the gauge quasi-static pressure $\hat{p}_{qs}$ of confined (unvented, non-breached) chambers subjected to internal blast loadings. This relationship relies on charge mass m_e, internal volume V_a and the fitting parameters η and C; being written as

$$\hat{p}_{qs} = C\left(\frac{m_e}{V_a}\right)^{\eta} \tag{6}$$

The slow relief of the internal pressure from vented structures was investigated by Anderson Jr et al. [12] who proposed a simple empirical relationship assuming an exponential decay from an initial peak gauge quasi-static pressure $\hat{p}_{qs}$ at local time $\tau = 0$. The relationship for the transient gauge quasi-static pressure p_{qs} is given by

$$p_{qs}(\tau) = \hat{p}_{qs}\exp\,(-k\tau) \tag{7}$$

where k is a fitting parameter. The parameters η, C and k can be obtained by applying standard regression methods (e.g. least squares) to test data.

3.1.2 Simplified analytical relationships

Feldgun et al. [14] proposed a simplified approach to simulate the residual pressure and the pressure relief of structures subjected to internal blast loadings. The derivation of their approach makes use of several assumptions to deliver equations that capture the relevant physics yet can be readily solved. Feldgun et al. [14] assumed that at the end of the non-stationary explosion response the gaseous detonation products can be treated as a perfect gas, the flow is barotropic and isentropic, the internal gas properties vary only with time, and density and pressure obey a Poisson's adiabatic process of the form

$$\frac{\overline{p}(t)}{p_a} = \left(\frac{\overline{\rho}(t)}{\rho_a}\right)^{\gamma} \tag{8}$$

which is an isentrope of the ideal gas equation of state. In the above equation t is absolute time, p_a is the ambient pressure, ρ_a is the ambient density, γ is the adiabatic index of the ambient air, $\overline{p}$ and $\overline{\rho}$ are the respective residual internal pressure and residual internal density for a partially confined explosion.

Based on those simplifications, an equation based on the energy conservation law was derived by Feldgun et al. [14] to find the residual pressure for a confined explosion. For obtaining the peak gauge quasi-static pressure $\hat{p}_{qs}$, this equation can be written as

$$\hat{p}_{qs} = \left(\frac{p_a}{\gamma - 1}(V_a - V_e) + m_e Q_e\right)\left(\frac{\overline{\gamma} - 1}{V_a}\right) - p_a \tag{9}$$

where $\overline{\gamma}$ is the adiabatic index of the blast products gaseous mixture; V_a is the internal volume of the enclosure; V_e is the volume of the explosive charge; m_e is the mass of the explosive charge; and Q_e is the explosive specific energy. The challenge resides on establishing the adiabatic index $\overline{\gamma}$ of the blast products gaseous mixture.

Internal blast loadings of vented or breached compartments are the most complicated to establish as computation of the pressure relief is complex and time dependent. Using the simplifications listed above, Feldgun et al. [14] introduced an approach with lumped parameters based on the Bernoulli equation that can adequately simulate the quasi-static pressure relief of vented structures.

At the onset of the blast explosion the flow through the vent relative to the energy release rate is insignificant [12]. The initial conditions at time t_0 of the quasi-static state for a vented confined explosion can then be assumed to be

$$\overline{m}(t_0) = \overline{\rho}(t_0)V_a = \rho_a V_a \left(\frac{\overline{p}(t_0)}{p_a}\right)^{1/\gamma} \tag{10}$$

$$\overline{p}(t_0) = \hat{p}_{qs} + p_a \tag{11}$$

where $\overline{m}$ is the mass of the blast products gaseous mixture filling the enclosure with internal volume V_a. The differential equation that describes the change with time of the mass of the gaseous blast products within the structure is given by

$$\frac{d\overline{m}}{dt} = -A_\Omega v_\Omega(t)\overline{\rho}(t) \tag{12}$$

The vent cross sectional area A_Ω is assumed to be constant throughout the blast process and the residual internal density $\overline{\rho}$ is defined as

$$\overline{\rho}(t) = \frac{\overline{m}(t)}{V_a} \tag{13}$$

The outflow velocity v_Ω through the vent is derived from the Bernoulli equation applied to the flow along a streamline through the vent domain Ω that when combined to Poisson's adiabate [Eq. (8)], yields

$$v_\Omega(t) = \sqrt{2\left(\frac{\gamma - 1}{\gamma}\right)\frac{p_a}{\rho_a}\left(\left(\frac{\overline{p}(t)}{p_a}\right)^{(1 - 1/\gamma)} - 1\right)} \tag{14}$$

Equations (8), (12)–(14) form a coupled system that is difficult to solve analytically but that can be promptly solved with an iterative numerical procedure using small discrete time steps. At the end of each time step, Eq. (8) can be employed to update the residual internal pressure $\overline{p}$.

3.2 Dynamic overpressure and the Friedlander–Heaviside series

Blast waves propagating towards surfaces and obstacles will be partially absorbed, reflected, diffracted, and refracted potentially multiple times. Such interactions complicate the description of the blast waveform due to the potential occurrence of numerous interferences of correlated shockwaves [36]. Current attempts to obtain the dynamic overpressure rely on numerical solutions of Euler's conservation laws coupled with the Jones–Wilkins–Lee (JWL) equation of state. This approach yields very accurate predictions at the expense of long turnaround times for complex three-dimensional cases even when extensive access to computational resources is available.

Idealised attempts currently available to describe pressure-time history using bi-linear pulses, lumped triangular pulses [17] or a Friedlander pulse of matching pressure-impulse [19] are not capable of describing the dynamic effects of reflected shockwaves and often display unmatching

peak arrival times and pressure magnitudes. Figure 3a presents a schematic representation of the dynamic overpressure-time history of reflected blast waves. From this figure it can be observed that each single pulse is similar in form to the Friedlander pulse discussed in Section 2. Assuming that the dynamic overpressure of reflected blast waves is a physically linear system formed by the combination of individual pulses obeying the superposition principle [36], the dynamic overpressure-time history can be deconstructed into individual Friedlander waveforms – as shown in Figure 3b-g for various local times τ_i for $i = 1,2 \ldots n$.

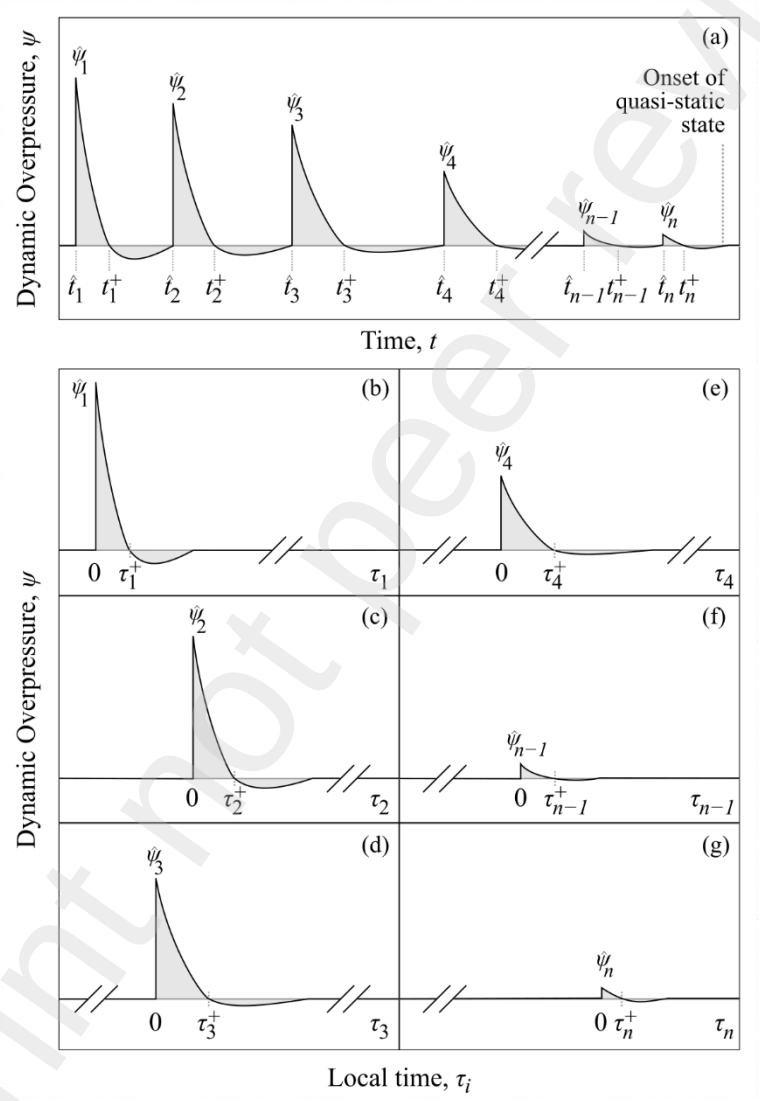

Figure 3. Schematic of the dynamic overpressure from a periodic blast wave. The complete overpressure-time history (a) is assumed to satisfy the superposition principle. Owing to the additivity property of this principle, the complex original system can be constructed by combining the responses from all simpler cases (b)–(g).

The Friedlander equation and its modifications are usually not defined at negative local times, i.e. at $\tau_i < 0$. One exception is the original version proposed by Friedlander in his seminal paper [32],

where the dynamic overpressure is considered null before the time of arrival, i.e. $\psi_i = 0$ for $\tau_i < 0$. This definition is necessary in order to develop a series capable of describing the total dynamic overpressure $\psi(t)$ for reflected bast waves.

The inclusion of the Heaviside step function into the modified Friedlander equation allows for a complete representation of the overpressure pulse over time. The Friedlander–Heaviside equation can thus be defined as the combination of the Heaviside step function $\mathrm{H}(\cdot)$ with the modified Friedlander equation (4) and a locally leveling static overpressure $\breve{\psi}_i$. The Friedlander–Heaviside equation to represent the dynamic overpressure ψ_i from each peak i becomes

$$\psi_i(\tau_i) = \mathrm{H}(\tau_i)\left(\hat{\psi}_i\left(1 - \frac{\tau_i}{\tau_i^+}\right)\exp\left(-\beta_i\tau_i\right) + \breve{\psi}_i\right) \tag{15}$$

for $i = 1,2,\ldots n$. Equation (15) allows for distinct local positive phase duration τ_i^+ and decay rate parameter β_i for each peak overpressure $\hat{\psi}_i$. The leveling static overpressure $\breve{\psi}_i$ ensures that the local dynamic overpressure pulse is aligned with the global dynamic overpressure.

To ensure that the peak dynamic overpressure $\hat{\psi}_i$ is maintained at $\tau_i = 0$, The Heaviside step function $\mathrm{H}(\cdot)$ is here defined as

$$\mathrm{H}(x) = \begin{cases} 1, & \text{if } x \geq 0 \\ 0, & \text{if } x < 0 \end{cases} \tag{16}$$

Strictly speaking, $\mathrm{H}(0)$ is not properly defined due to the characteristic discontinuity of step functions [37, 38].

Applying the superposition principle on n Friedlander–Heaviside curves generated with Eq. (15), the global dynamic overpressure-time history $\psi(t)$ becomes

$$\begin{aligned}\psi(t) = &\left(\hat{\psi}_1\left(1 - \frac{\tau_1}{\tau_1^+}\right)\exp\left(-\beta_1\tau_1\right) + \breve{\psi}_1\right)\mathrm{H}(\tau_1) + \left(\hat{\psi}_2\left(1 - \frac{\tau_2}{\tau_2^+}\right)\exp\left(-\beta_2\tau_2\right) + \breve{\psi}_2\right)\mathrm{H}(\tau_2) + \ldots \\ &+ \left(\hat{\psi}_n\left(1 - \frac{\tau_n}{\tau_n^+}\right)\exp\left(-\beta_n\tau_n\right) + \breve{\psi}_n\right)\mathrm{H}(\tau_n)\end{aligned} \tag{17}$$

which can be rewritten in compact notation as

$$\psi(t) = \sum_{i=1}^{n}\left(\breve{\psi}_i + \hat{\psi}_i\left(1 - \frac{\tau_i}{\tau_i^+}\right)\exp\left(-\beta_i\tau_i\right)\right)\mathrm{H}(\tau_i) \tag{18}$$

Equation (18) is a simplified phenomenological description of the dynamic overpressure of reflected blast waves. Preliminary evaluations of this equation have shown that curve i may have an offsetting

effect on the local Friedlander–Heaviside curve $i+1$, increasing the difficulty in obtaining an optimum global fit. To address this shortcoming, the argument in the Heaviside step function can be replaced by a quadratic function to establish the applicable duration $\check{\tau}_i$ of curve i. The final form of the Friedlander–Heaviside series for describing the dynamic overpressure over time $\psi(t)$ is thus given by

$$\psi(t) = \sum_{i=1}^{n} \left(\check{\psi}_i + \hat{\psi}_i \left(1 - \frac{\tau_i}{\tau_i^+} \right) \exp\left(-\beta_i \tau_i \right) \right) \mathrm{H}\left(\frac{\tau_i}{\check{\tau}_i} - \frac{\tau_i^2}{\check{\tau}_i^2} \right) \tag{19}$$

The absolute time parameters may be converted to local time parameters by using

$$\tau_i = t - \hat{t}_i, \quad \tau_i^+ = t_i^+ - \hat{t}_i, \quad \check{\tau}_i = \check{t}_i - \hat{t}_i \tag{20}$$

where $\hat{t}_i$ is the time of arrival of peak i, t_i^+ is the time at which the positive phase of peak i ends, and $\check{t}_i$ is the time at which the local pressure pulse i is no longer valid.

The complete pressure-time history $p(t)$ of reflected blast waves can be obtained by combining the dynamic overpressure $\psi(t)$ with the residual pressure $\overline{p}(t)$, that is

$$p(t) = \psi(t) + \overline{p}(t) \tag{21}$$

Selected cases are presented in the next section to demonstrate Eq. (21) ability to describe the pressure-time history of reflected blast waves.

4 Selected applications of the Friedlander–Heaviside series

The Friedlander–Heaviside series is fitted to selected cases available in the literature to illustrate its ability to represent periodic blast waves. These cases were chosen as they cover common situations where reflected blast waves occur. The examples below aim at replicating the pressure-time history of detonations in a built environment (Section 4.1) and of internal blast loading in unvented (Section 4.2) and vented (Section 4.3) structures.

To find the most suitable parameters for the Friedlander–Heaviside series the following procedure was utilised:

- Identify n pressure peaks of interest
- For each peak $i = 1,2 \ldots n$ estimate rough values of:
    - the overpressure peak $\hat{\psi}_i$,
    - the leveling static overpressure $\check{\psi}_i$
    - the time of arrival $\hat{t}_i$,

- the time at which the positive phase ends t_i^+,
- the time at which the local pressure pulse is no longer valid $\check{t}_i$
- the decay coefficient β_i

- Map absolute time to local time using Eq. (20)
- Employ a suitable optimisation algorithm (e.g. least squares, differential evolution) to obtain optimal Friedlander–Heaviside coefficients using the estimated values as initial guesses
- Compute the quasi-static pressure p_{qs} relevant to the system
- Calculate the residual pressure $\overline{p}$ using Eq. (5)
- Recover the complete pressure-time history $p(t)$ of reflected blast waves using Eqs. (19) and (21)

4.1 Blast propagating in an urban environment

Explosions in urban environments are enhanced by shockwave reflections resulting from interactions with the surrounding buildings. Full-scale experimental testing contemplating explosions in urban scenarios is restrained by high associated costs and extremely hazardous aspects of such events. Scaled experiments offer feasible testing options which can be used to predict larger scale blast events [39].

To better understand the propagation of blast waves in urban environments, Fouchier et al. [3] performed a series of non-destructive small scale (1:200) experimental tests. An example considered by these authors is used here to demonstrate the ability of the Friedlander–Heaviside series [Eq. (19)] to describe the pressure-time history caused by reflected blast waves in urban environments. The selected test case measured the detonation of an explosive charge consisting of 0.08g of pentaerythritol tetranitrate (PETN) and 1031g of cyclotrimethylenetrinitramine (RDX) in a 250mm wide straight street surrounded by 100mm tall buildings. The gauging sensor is located at a distance of 350mm from the charge centre. Figure 4 provides a schematic view of the test case.

Five different Friedlander–Heaviside series were generated to verify the improvement in accuracy with an increasing n. The Friedlander–Heaviside coefficients for Eq. (19) were obtained using differential evolution optimisation [40] and are listed in Table 1. Remember that the Friedlander–Heaviside series uses a local coordinate system which is then mapped to global values. The apparently high values of $\hat{\psi}_i$ (third column of Table 1) are compensated by the leveling values of $\check{\psi}_i$ (last column of Table 1). Figure 5 presents a comparison between the measured overpressure-time history test results from Fouchier et al. [3] and the Friedlander–Heaviside series for $n =$ 1, 2, 3, 4 and 5. This figure also highlights the improvement in accuracy as quantified by the coefficient of determination R^2, which improves with an increasing n. From Figure 5 it can be observed that the

Friedlander–Heaviside series can rather adequately describe the overpressure-time history when, as expected, a sufficient number n of overpressure peaks are utilised.

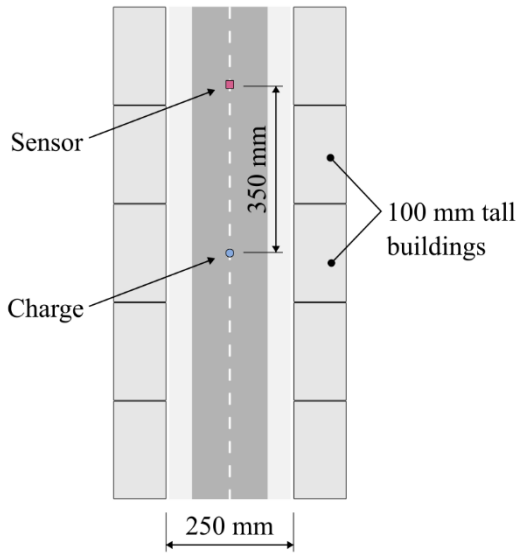

Figure 4. Schematic of scaled blast in an urban street surrounded by buildings as considered by Fouchier et al. [3].

Table 1. Friedlander–Heaviside coefficients for describing the overpressure-time history measured at 350mm from the centre of explosion in a scaled urban street.

n	i	$\hat{\psi}_i$ [kPa]	β_i [ms^{-1}]	τ_i^+ [ms]	$\hat{t}_i$ [ms]	$\check{t}_i$ [ms]	$\check{\psi}_i$ [kPa]
1	1	193.668	0.593	9.752	1.182	9.575	-42.272
2	1	194.364	0.266	2.573	1.187	4.107	-42.272
	2	82.803	1.091	6.288	4.107	9.575	-39.018
3	1	114.056	2.150	0.676	1.187	1.775	32.774
	2	194.364	0.936	1.895	1.775	4.107	-42.272
	3	82.803	1.091	6.288	4.107	9.575	-39.018
4	1	114.056	2.150	0.676	1.187	1.775	32.774
	2	194.364	0.936	1.895	1.775	4.107	-42.272
	3	82.803	1.247	2.655	4.107	6.416	-39.018
	4	18.778	1.358	3.633	6.416	9.575	-14.169
5	1	114.056	2.150	0.676	1.187	1.775	32.774
	2	194.364	0.971	1.982	1.775	4.107	-42.272
	3	82.803	1.247	2.655	4.107	6.416	-39.018
	4	18.778	1.505	2.384	6.416	8.489	-14.169
	5	3.382	2.747	13.238	8.489	11.000	-7.027

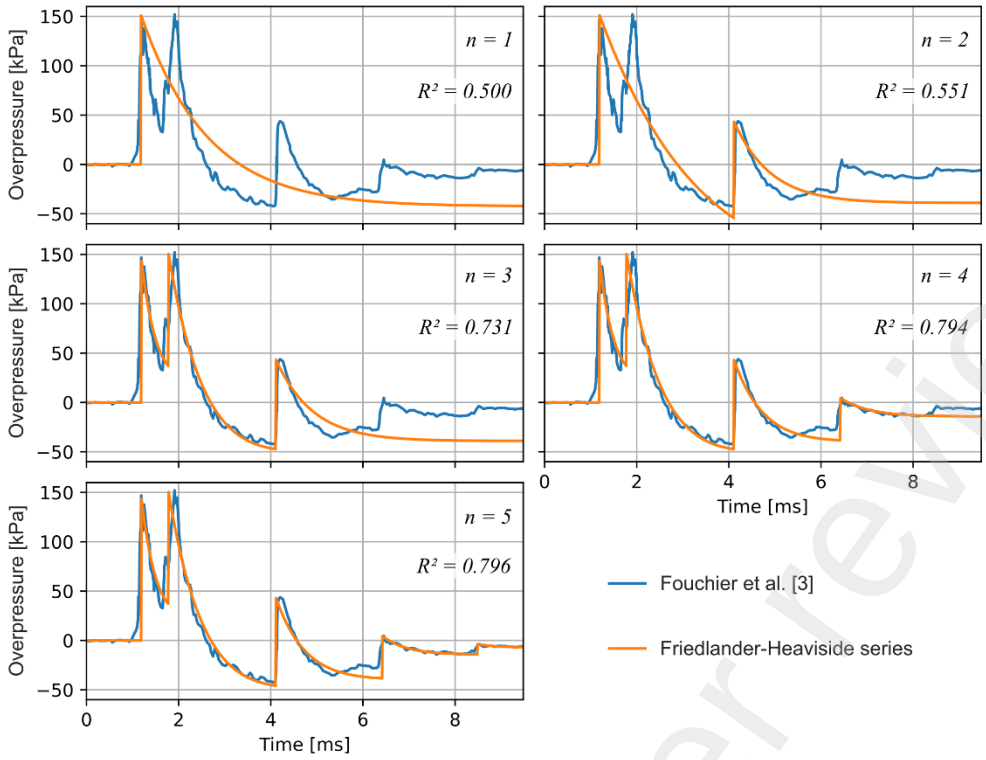

Figure 5. Comparison of different Friedlander–Heaviside series against measured overpressure-time history at a distance of 350mm from the centre of detonation in a scaled urban street surrounded by buildings. Increasing n improves the accuracy of the Friedlander–Heaviside series.

4.2 Container under internal blast loading

The multiple reflections of shockwaves present in internal blasting scenarios increase the complexities of describing pressure-time history. In an effort aimed at better understanding structural response and failure mechanisms of confined detonations, Pickerd et al. [22] conducted a series of small scale internal blast experiments of 1 m³ welded steel containers. The detonations were initiated by plastic explosive (PE4) charges centrally located within the container. Pressure-time histories were captured by sensors located at the edge and at corner of the container. An overview of the experimental set up is illustrated in Figure 6. The experimental results from detonated cylindrical charges of (Case 1) 345 g (height and diameter of 65 mm) and (Case 2) 431 g (height and diameter of 70mm) were here utilised for evaluating the Friedlander–Heaviside series performance in internal blast loading scenarios. Table 2 gives additional information concerning the initial conditions.

Table 2. Initial conditions for a 1m³ steel container subjected to internal blast from a PE4 charge

ρ_a [kg/m³]	p_a [kPa]	γ	ρ_e [kg/m³]	Q_e [J/g]	$\overline{\gamma}$
1.225	100	1.4	1600	6700	1.4

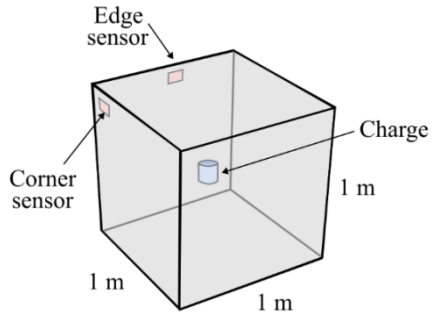

Figure 6. Schematic of container subjected to internal blast as investigated by Pickerd et al. [22].

The dynamic overpressure-time history was created by subtracting the quasi-static pressure (calculated using Eq. (9)) from the experimental data. The Friedlander–Heaviside coefficients for Eq. (19) were then calculated via differential evolution optimisation [40]. Tables 3 and 4 list the coefficients for constructing the pressure-time history as measured at the edge and corner sensors for Case 1 (Table 3) and Case 2 (Table 4). The Friedlander–Heaviside pressure-time history curves generated with those coefficients are compared against corresponding experimental results in Figure 7 (Case 1) and Figure 8 (Case 2). These figures demonstrate the overall good correlation between experimental measurements and the Friedlander–Heaviside curves of the pressure-time history, further corroborated by the strong agreement between experimental and Friedlander–Heaviside impulse curves.

Table 3. Friedlander–Heaviside coefficients for describing the overpressure-time history for a 1m³ steel container under internal detonation caused by a 345g cylindrical charge.

Sensor	i	$\hat{\psi}_i$ [MPa]	β_i [ms^{-1}]	τ_i^+ [ms]	$\hat{t}_i$ [ms]	$\check{t}_i$ [ms]	$\check{\psi}_i$ [MPa]
Edge	1	1.275	0.000	0.038	0.282	0.315	-0.526
	2	1.414	5.000	0.137	0.276	0.390	-0.665
	3	0.368	0.000	0.055	0.390	0.450	-0.530
	4	2.646	3.561	0.258	0.451	0.697	-0.525
	5	0.199	0.000	0.112	0.697	0.803	-0.769
	6	0.461	5.000	0.100	0.803	0.890	-0.909
	7	0.399	0.016	0.023	0.890	0.915	-0.709
	8	1.452	1.006	0.172	0.920	1.120	-0.415
	9	0.237	0.000	0.068	1.120	1.200	-0.543
	10	0.191	0.000	0.115	1.200	1.319	-0.650
	11	0.172	5.000	0.088	1.350	1.439	-0.072
	12	0.952	0.000	0.510	1.439	1.895	-0.664
	13	1.299	1.911	0.418	1.895	2.360	-0.736
	14	0.087	0.500	0.332	2.360	2.516	-0.649
Corner	1	1.043	2.846	0.118	0.336	0.444	-0.925
	2	1.991	0.000	0.044	0.524	0.565	2.986
	3	6.301	5.000	0.457	0.565	1.280	-1.041
	4	1.986	2.166	0.315	1.475	1.821	-0.464
	5	0.877	5.000	0.427	1.821	2.325	-1.167
	6	0.666	5.000	6.524	2.325	2.500	-1.190

Table 4. Friedlander–Heaviside coefficients for describing the overpressure-time history for a 1m³ steel container under internal detonation caused by a 431g cylindrical charge.

Sensor	i	$\hat{\psi}_i$ [MPa]	β_i [ms^{-1}]	$\tau_i^{\dagger}$ [ms]	$\hat{t}_i$ [ms]	$\check{t}_i$ [ms]	$\check{\psi}_i$ [MPa]
Edge	1	1.650	5.000	0.137	0.259	0.400	-0.954
	2	5.554	5.000	0.068	0.420	0.500	0.668
	3	1.614	4.398	0.380	0.500	0.830	-1.117
	4	1.492	5.000	0.094	0.830	0.941	-0.125
	5	1.329	5.000	0.468	0.941	1.410	-0.785
	6	1.463	5.000	0.264	1.410	1.720	-0.577
	7	0.810	0.000	0.094	1.720	1.810	-0.699
	8	1.801	5.000	0.656	1.810	2.390	-0.725
	9	0.465	0.500	0.306	2.390	2.516	-0.640
Corner	1	7.689	2.169	0.036	0.405	0.436	-0.054
	2	8.774	5.000	0.030	0.436	0.470	5.842
	3	3.774	0.000	0.023	0.470	0.490	6.255
	4	6.898	5.000	0.089	0.490	0.595	1.190
	5	2.384	5.000	0.132	0.595	0.750	-0.445
	6	0.520	5.000	0.192	0.750	1.270	-1.116
	7	0.568	5.000	1.10×10^{4}	1.270	1.400	-1.178
	8	4.217	5.000	0.297	1.400	1.720	-0.395
	9	0.269	5.000	0.077	1.720	1.810	-0.654
	10	0.323	5.000	0.216	1.810	2.250	-1.164
	11	0.854	5.000	0.090	2.250	2.356	-1.175
	12	0.342	5.000	1.10×10^{4}	2.356	2.450	-1.150
	13	0.500	0.500	0.255	2.450	2.516	-0.777

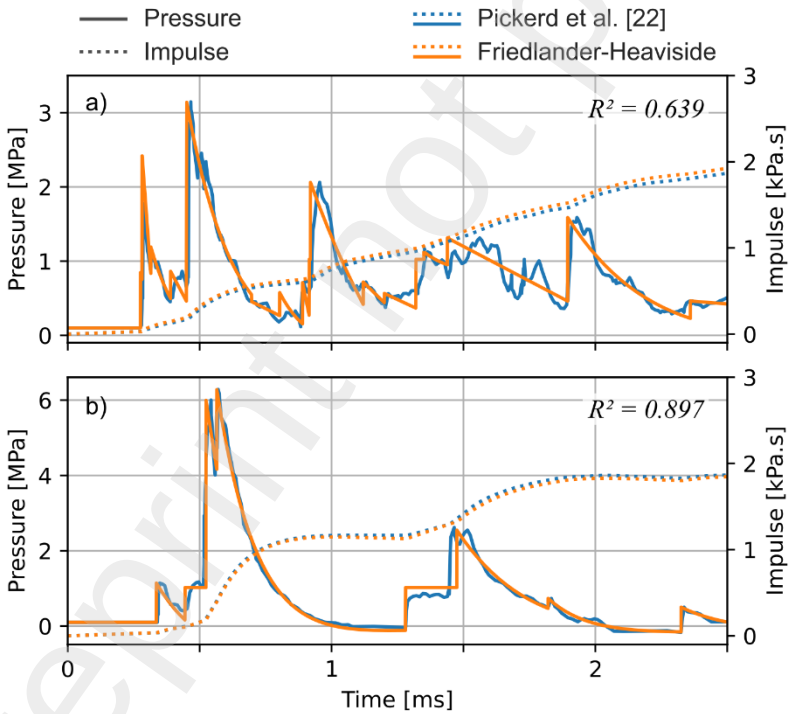

Figure 7. Pressure-time history (solid lines) measured at (a) edge and (b) corner sensors for 345g PE4 cylindrical charges detonated within 1m³ steel containers (Case 1) contrasted to respective Friedlander–Heaviside curves. Reasonable agreement is observed as quantified by the coefficients of determination R². The impulse (dashed lines) computed from the Friedlander–Heaviside curves also agrees well with the corresponding experimental impulse.

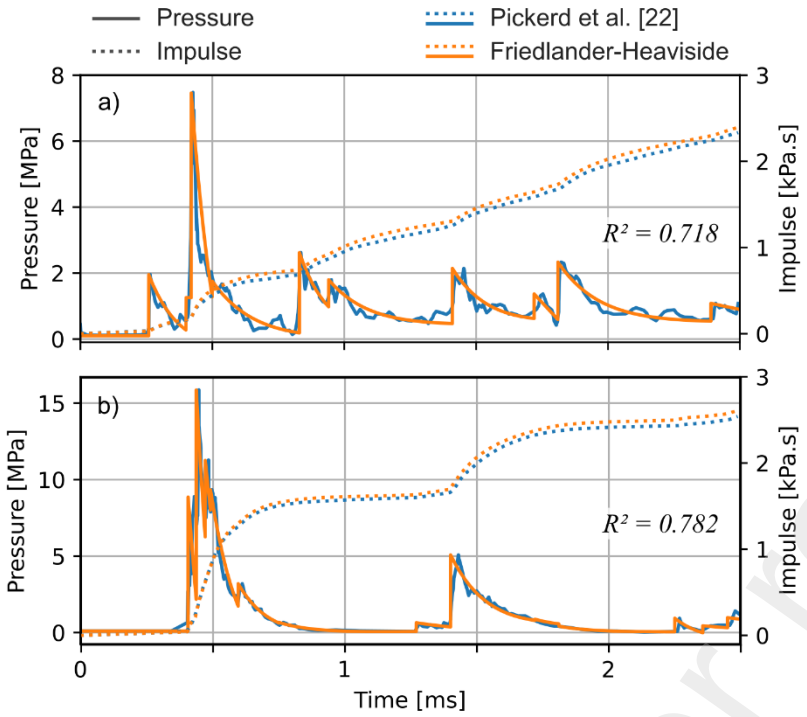

Figure 8. Pressure-time history (solid lines) measured at (a) edge and (b) corner sensors for 431g PE4 cylindrical charges detonated within 1m³ steel containers (Case 2) contrasted to respective Friedlander–Heaviside curves. Adequate agreement is observed as quantified by the coefficients of determination R². The impulse (dashed lines) computed from the Friedlander–Heaviside curves also agrees well with the corresponding experimental impulse.

4.3 Internal detonation in a partially vented cylindrical chamber

Venting affects the overall mechanical response to internal blast loading as it allows for an almost immediate pressure relief as the quasi-static state of the explosion slowly decays until eventually reaching the external ambient state. The Friedlander–Heaviside series capacity for describing the pressure-time history of confined explosions of vented structures is assessed against numerical simulations results from Feldgun et al. [15]. In these simulations a circular duct with cross sectional area of 0.053m² and length of 2800mm is attached to a cylindrical chamber with a volume of 0.38485m³ which is subjected to the internal explosion of 1.1kg of a cylindrical PETN charge, as shown in Figure 9. Four venting conditions were considered, namely (a) no venting and circular venting of (b) 100mm radius, (c) 130mm radius, and (d) 190mm radius. Other relevant considerations about the initial conditions of the problem are given in Table 5.

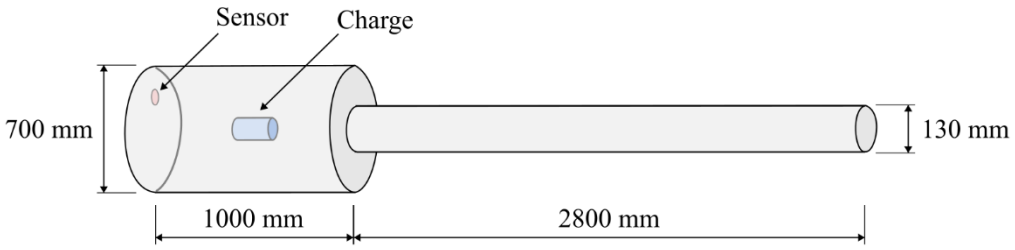

Figure 9. Partially vented cylindrical chamber subjected to internal blast loading as numerically simulated by Feldgun et al. [15]. The sensor is placed 160mm from the cylinder wall.

Table 5. Initial conditions of a vented cylindrical chamber subjected to internal blast from a PETN charge

ρ_a [kg/m³]	p_a [kPa]	γ	ρ_e [kg/m³]	m_e [kg]	Q_e [J/g]	$\overline{\gamma}$
1.225	100	1.4	1770	1.10	5860	1.45

The analytical method described in Section 3.1.2 was employed to separate the quasi-static pressure and the dynamic overpressure from pressure-time histories obtained by Feldgun et al. [15]. The Friedlander–Heaviside series [Eq. (19)] was then fitted to the dynamic overpressure-time histories using differential evolution optimisation [40]. Table 6 lists the Friedlander–Heaviside coefficients obtained for all four cases investigated by Feldgun et al. [15]. The fitted pressure-time histories given by Figure 10 were then retrieved by employing Eq. (21).

The results in Figure 10 show that the combined Friedlander–Heaviside series and Feldgun et al.'s method [14] allowed for a sensible description of the pressure-time histories computed via numerical simulations. This figure also shows that the pressure impulse computed from Friedlander–Heaviside curve is once more accurately matched to the respective numerical impulse.

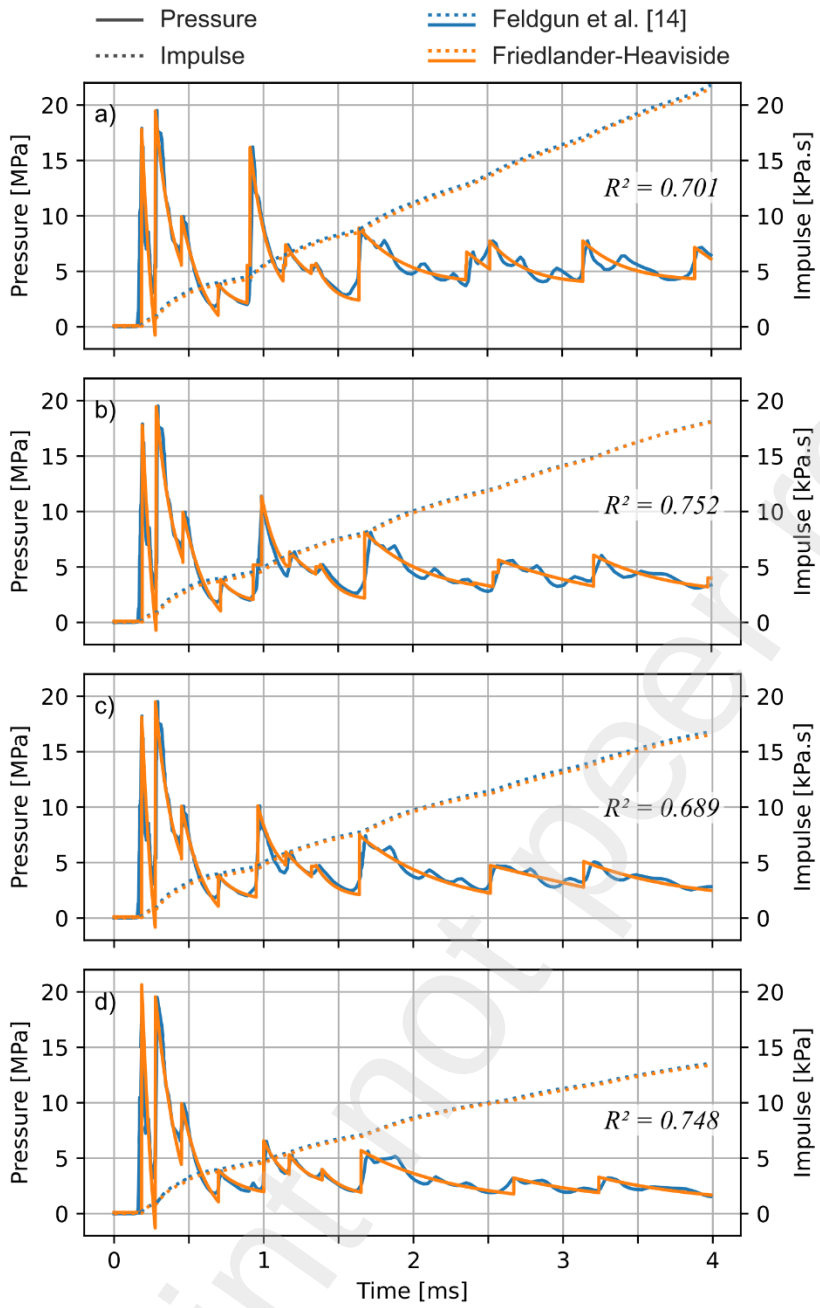

Figure 10. Pressure-time histories (solid lines) for internal explosion of 1.1kg PETN charge in a cylindrical chamber considering (a) no venting, as well as circular venting with (b) 100mm radius, (c) 130mm radius, and (d) 190mm radius. Experimental tests are overlayed by Friedlander–Heaviside curves. Reasonable agreement was obtained, as demonstrated by the coefficients of determination R^2. It can also be observed a good correlation between the impulse computed from the Friedlander–Heaviside curves and the corresponding numerical impulse (dashed lines).

Table 6. Friedlander–Heaviside coefficients for a vented cylindrical chamber subjected to internal blast

Vent radius	i	$\hat{\psi}_i$ [MPa]	β_i [ms^{-1}]	τ_i^+ [ms]	$\hat{t}_i$ [ms]	$\check{t}_i$ [ms]	$\check{\psi}_i$ [MPa]
-	1	14.817	5.000	0.064	0.184	0.275	-2.478
	2	14.148	5.000	0.186	0.276	0.450	-0.194
	3	8.126	3.146	0.204	0.451	0.697	-3.743
	4	1.613	5.000	0.165	0.697	0.890	-3.296
	5	12.062	5.000	0.220	0.910	1.131	-1.397
	6	2.170	2.777	0.129	1.148	1.319	-0.313
	7	2.852	5.000	0.173	1.350	1.639	-2.694
	8	4.714	2.053	0.735	1.639	2.355	-1.352
	9	3.049	0.500	0.332	2.360	2.516	-1.856
	10	3.681	2.890	0.672	2.516	3.138	-1.497
	11	3.481	2.576	0.853	3.138	3.887	-1.285
	12	1.169	0.000	0.123	3.887	5.000	0.442
100mm	1	14.780	5.000	0.064	0.184	0.275	-2.440
	2	14.152	5.000	0.186	0.276	0.450	-0.146
	3	8.024	3.190	0.204	0.451	0.697	-3.501
	4	1.554	5.000	0.165	0.697	0.910	-2.977
	5	6.105	5.000	0.157	0.965	1.131	0.103
	6	1.642	1.832	0.137	1.148	1.319	-0.360
	7	2.497	4.939	0.173	1.350	1.639	-2.271
	8	4.321	1.604	0.654	1.639	2.355	-1.050
	9	0.724	0.500	0.336	2.355	2.480	-1.731
	10	2.230	0.606	0.671	2.516	3.138	-1.110
	11	2.728	1.360	0.853	3.138	3.887	-0.925
130mm	1	15.085	5.000	0.064	0.184	0.275	-2.414
	2	14.165	5.000	0.186	0.276	0.450	-0.113
	3	8.103	3.469	0.203	0.451	0.697	-3.341
	4	1.729	5.000	0.223	0.697	0.950	-2.981
	5	5.330	5.000	0.203	0.961	1.140	-0.134
	6	1.915	1.415	0.151	1.148	1.319	-0.739
	7	2.111	5.000	0.173	1.350	1.639	-2.011
	8	4.422	1.075	0.760	1.639	2.516	-1.429
	9	1.717	0.129	0.661	2.516	3.138	-0.901
	10	2.216	0.997	0.853	3.138	5.000	-0.704
190mm	1	17.340	5.000	0.064	0.184	0.275	-2.178
	2	15.427	3.059	0.186	0.276	0.450	-1.265
	3	7.755	3.322	0.203	0.451	0.697	-2.900
	4	1.562	5.000	0.349	0.697	1.000	-2.349
	5	3.268	5.000	0.255	1.000	1.170	-0.971
	6	1.767	4.388	0.161	1.170	1.390	-0.502
	7	1.695	5.000	0.221	1.390	1.650	-1.488
	8	3.162	1.280	1.208	1.650	2.670	-0.970
	9	1.031	1.069	0.667	2.670	3.238	-0.426
	10	1.201	0.982	0.738	3.238	5.000	-0.146

5 Conclusion

Reflected blast waves are often observed in confined detonations and in explosions in urban settings. The semi-empirical methods currently available to describe the pressure-time history of reflected blast waves are overly simplified and focus mostly on providing equivalent pressure-impulse approximations. Comprehensive numerical methods based on Euler's conservation laws can provide accurate estimates of complex shockwave interactions with surfaces and obstacles at the expense of long lead times and costly computational resources.

Aimed at developing a simple phenomenological model for describing the dynamic overpressure-time history of reflected blast waves, a novel Friedlander–Heaviside series was presented and applied to selected cases found in the literature. This series was obtained by combining the well-known Friedlander equation with the Heaviside step function and applying the superposition principle. After obtaining the necessary parameters, the Friedlander–Heaviside series can be employed along with advanced structural models for calculating detailed estimates of structural response to reflected blast loadings.

The combination of the Friedlander–Heaviside series with models readily available for predicting the residual quasi-static pressure provide for an efficient tool that allows the complete description of pressure-time histories from reflected blast events. This series can potentially also be applied to describe secondary pressure peaks originating from afterburning effects. Comparisons of the novel Friedlander–Heaviside series curves to experimental and numerical results available in the literature demonstrate that in overall this series can rather adequately describe the complex waveform of reflected blast waves.

Acknowledgements

This paper includes research that was supported by DMTC Limited (Australia). The author has prepared this paper in accordance with the intellectual property rights granted to partners from the original DMTC project. The author is also grateful to Dr Alexander Gargano and Vanessa Pickerd of Defence Science and Technology Group (Australia) for their comments and helpful discussions.

References

1. Gelfand, B.E., et al., *Specific features of incident and reflected blast waves.* Shock Waves, 1994. **4**(3): p. 137-143.

2. Kleine, H., E. Timofeev, and K. Takayama, *Reflection of blast waves from straight surfaces*, in *Shock Waves*, Z. Jiang, Editor. 2005, Springer Berlin Heidelberg: Berlin, Heidelberg. p. 1019-1024.
3. Fouchier, C., et al., *Experimental investigation of blast wave propagation in an urban environment.* Journal of Loss Prevention in the Process Industries, 2017. **49**: p. 248-265.
4. Remennikov, A.M., *Evaluation of blast loads on buildings in urban environment*, in *Structures Under Shock and Impact VIII*, N. Jones and C.A. Brebbia, Editors. 2004, WIT Press: Ashurst, Hampshire, England. p. 73-82.
5. Johansson, M., O. Larsen, and L. Laine. *EXPERIMENTS AND ANALYSES OF EXPLOSION AT AN URBAN INTERSECTION*. in *20th International Symposium on Military Aspects of Blast and Shock*. 2008. Oslo, Norway: Spiez Laboratory (Spiezbase).
6. Remennikov, A.M., *A review of methods for predicting bomb blast effects on buildings.* Journal of Battlefield Technology, 2003. **6**(3): p. 5-10.
7. Remennikov, A.M. and T.A. Rose, *Modelling blast loads on buildings in complex city geometries.* Computers & Structures, 2005. **83**(27): p. 2197-2205.
8. Rose, T.A., *Influence of the principal geometrical parameters of straight city streets on positive and negative phase blast wave impulses.* International journal of impact engineering, 2002. **27**(4): p. 359-376.
9. Smith, P.D. and T.A. Rose, *Blast wave propagation in city streets—an overview.* Progress in Structural Engineering and Materials, 2006. **8**(1): p. 16-28.
10. Isaac, O.S., et al., *Blast wave interaction with structures – An overview.* International Journal of Protective Structures, 2022: p. 20414196221118595.
11. Marks, N.A., et al., *Airblast variability and fatality risks from a VBIED in a complex urban environment.* Reliability Engineering & System Safety, 2021. **209**: p. 107459.
12. Anderson Jr, C.E., et al., *Quasi-static pressure, duration, and impulse for explosions (e.g. HE) in structures.* International Journal of Mechanical Sciences, 1983. **25**(6): p. 455-464.
13. Weibull, H.R.W., *Pressures Recorded in Partially Closed Chambers at Explosion of TNT Charges.* Annals of the New York Academy of Sciences, 1968. **152**(1): p. 357-361.
14. Feldgun, V.R., Y.S. Karinski, and D.Z. Yankelevsky, *A simplified model with lumped parameters for explosion venting simulation.* International Journal of Impact Engineering, 2011. **38**(12): p. 964-975.
15. Feldgun, V.R., et al., *Prediction of the quasi-static pressure in confined and partially confined explosions and its application to blast response simulation of flexible structures.* International Journal of Impact Engineering, 2016. **90**: p. 46-60.
16. Chan, P.C. and H.H. Klein, *A Study of Blast Effects Inside an Enclosure.* Journal of Fluids Engineering, 1994. **116**(3): p. 450-455.
17. Dragos, J., C. Wu, and D.J. Oehlers, *Simplification of fully confined blasts for structural response analysis.* Engineering Structures, 2013. **56**: p. 312-326.
18. Dragos, J., C. Wu, and K. Vugts, *Pressure-Impulse Diagrams for an Elastic-Plastic Member under Confined Blasts.* International Journal of Protective Structures, 2013. **4**(2): p. 143-162.
19. Levine, J., J.P. Dionne, and A. Makris. *INTERNAL BLAST CONSIDERATIONS IN EXPLOSIVE-FORCED ENTRY*. in *25th International Symposium on Military Aspects of Blast and Shock*. 2018. The Hague, Netherlands: Spiez Laboratory (Spiezbase).
20. Hu, Y., et al., *Characteristics of Confined Blast Loading in Unvented Structures.* International Journal of Protective Structures, 2011. **2**(1): p. 21-43.
21. Kinney, g.F., R.G.S. Sewell, and K.J. Graham, *Peak Overpressures for Internal Blast*. 1979, NAVAL WEAPONS CENTER CHINA LAKE CA.
22. Pickerd, V., et al., *Analysis of the structural response and failure of containers subjected to internal blast loading.* International Journal of Impact Engineering, 2016. **95**: p. 40-53.
23. Saleh, M., et al. *Optimisation of numerical modelling for structures subjected to internal blast*. in *25th International Symposium on Military Aspects of Blast and Shock*. 2018. Spiez Laboratory (Spiezbase).

24. Salvado, F.C., et al., *Confined explosions: The effect of compartment geometry.* Journal of Loss Prevention in the Process Industries, 2017. **48**: p. 126-144.
25. Wu, C., *Experimental and numerical investigation of confined explosion in a blast chamber.* Journal of loss prevention in the process industries, 2013. **26**(4): p. 737-750.
26. Zhang, C., P.J. Tan, and Y. Yuan, *Confined blast loading of steel plates with and without pre-formed holes.* International Journal of Impact Engineering, 2022. **163**: p. 104183.
27. Yao, S., et al., *Equivalent scaling method on the dynamic response of box-shaped structures under internal blast.* International Journal of Impact Engineering, 2022. **160**: p. 104074.
28. Bortolan Neto, L., et al., *Rapid mechanical evaluation of quadrangular steel plates subjected to localised blast loadings.* International Journal of Impact Engineering, 2020. **137**: p. 103461.
29. Fedkiw, R.P., et al., *A Non-oscillatory Eulerian Approach to Interfaces in Multimaterial Flows (the Ghost Fluid Method).* Journal of Computational Physics, 1999. **152**(2): p. 457-492.
30. Boscarino, S., L. Pareschi, and G. Russo, *Implicit-Explicit Runge--Kutta Schemes for Hyperbolic Systems and Kinetic Equations in the Diffusion Limit.* SIAM Journal on Scientific Computing, 2013. **35**(1): p. A22-A51.
31. Hansen, O.R., et al., *Using computational fluid dynamics (CFD) for blast wave predictions.* Journal of Loss Prevention in the Process Industries, 2010. **23**(6): p. 885-906.
32. Friedlander, F.G. and G.I. Taylor, *The diffraction of sound pulses I. Diffraction by a semi-infinite plane.* Proceedings of the Royal Society of London. Series A. Mathematical and Physical Sciences, 1946. **186**(1006): p. 322-344.
33. Dewey, J.M., *The Friedlander Equations*, in *Blast Effects: Physical Properties of Shock Waves*, I. Sochet, Editor. 2018, Springer International Publishing: Cham. p. 37-55.
34. Dewey, J.M., *The shape of the blast wave: studies of the friedlander equation*, in *21st Military Aspects of Blast and Schock Symposium (MABS 21)*. 2010, Spiez Laboratory (Spiezbase): Jerusalem, Israel. p. 9.
35. Ngo, T., et al., *Blast loading and blast effects on structures – an overview.* Electronic Journal of Structural Engineering, 2007. **7**: p. 76–91.
36. Freegarde, T., *Introduction to the Physics of Waves*. 2012, Cambridge: Cambridge University Press.
37. Iliev, A., N. Kyurkchiev, and S. Markov, *On the approximation of the step function by some sigmoid functions.* Mathematics and Computers in Simulation, 2017. **133**: p. 223-234.
38. Legua, M.P., I. Morales, and L.M. Sánchez Ruiz. *The Heaviside Step Function and MATLAB*. 2008. Springer.
39. Baker, W.E., *Blast Pressure Effects: An Overview*, in *Design Considerations for Toxic Chemical and Explosives Facilities*, R.A. Scott Jr and L.J. Doemeny, Editors. 1987, American Chemical Society: Washington D.C. p. 2-57.
40. Price, K.V., R.M. Storn, and J.A. Lampinen, *Differential evolution: a practical approach to global optimization*. Natural computing series. 2005, Berlin ; New York: Springer. 538.